

true for exotic fuels such as proton-Boron or Helium-3, as the Z^2 increase in Bremsstrahlung for these reactions would be compensated to some degree by the increased energy per fusion event.

II. DERIVATION OF ENERGY GAIN AND LOSS EXPRESSIONS

A. Device geometry and operation

We will examine the simple grid arrangement consisting of two coaxial negatively biased rings within a grounded cylindrical vacuum chamber as shown in Fig.2, which has been shown [19–21] to give IEC plasma properties. This grid replaces the cathode shown in Fig.1.

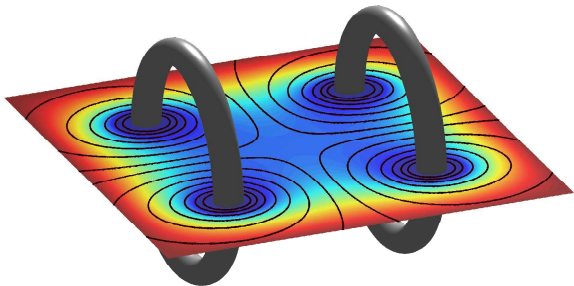


FIG. 2: Two-ring cathode grid with embedded magnetic field coils that produce a magnetic cusp. Magnetic field lines are in black; electric potential is shown as a heatmap with blue representing a negative potential and red representing a ground (a grounded cylindrical chamber is implicit at the edges of the diagram)

Current-carrying coils are embedded within each ring and electrically isolated from it. Current circulates in opposite directions in each coil so as to produce opposing magnetic fields. The magnetic field created by the coils will be shown to shield the surface of the rings from ion impact. Moreover, the opposing currents create a magnetic null at the midpoint of the axis through the rings, point cusps at the center of each ring, and a line cusp in a plane that bisects the axis at right angles.

The purpose of this magnetic configuration is to increase the ion density beyond the limit imposed by a concentration of only positive charges. Trapping electrons in this cusped geometry, such that their density is lower than those of the ions, enables the ion density to be increased while maintaining the net positive charge on the non-neutral plasma. This increase in ion density will enable an increase in fusion density. Although electrons are not needed in order to show a net energy gain, they enable an increase in the net energy produced for

practical considerations.

In general, the device is similar to a spindle cusp arrangement but with a negative voltage bias imposed on the rings. Although other grid configurations can be used, the arrangement shown here has cylindrical symmetry that makes analysis and construction relatively straightforward.

In the following subsections we will quantify the various energy gain and loss mechanisms, then finally integrate all of them to illustrate a net fusion energy gain.

B. Density profiles and fusion power

The conserved quantities (constants of the motion) for our system are the total energy, H , and the z -component of angular momentum, L_z , which correspond to time- and rotation-invariance, respectively. In cylindrical polar coordinates (r, θ, z) with z the axis of symmetry, we have:

$$H = \frac{1}{2}m(v_r^2 + v_z^2 + v_\theta^2) + q\phi \quad (1)$$

$$L_z = r(mv_\theta + qA_\theta), \quad (2)$$

where ϕ is the electric potential and A_θ is the only non-vanishing component of the magnetic vector potential for our system. Density variation emerges through the position-dependence of A_θ and ϕ . L_z is seen to suppress density around the $r = 0$ axis.

Where the magnetic field is slowly-changing over distance scales of order of the gyroradius, we have a third (“adiabatic”) invariant: $\mu \approx \frac{mv_\perp^2}{2B}$, v_\perp is the component of particle velocity perpendicular to the local magnetic field. Adiabaticity will tend to reduce cusp losses [38]; we will assume for the sake of conservatism that our plasma is nonadiabatic.

Since any function whose only arguments are constants of the motion is a stationary solution to the Vlasov equation, we can write electron and ion distribution functions in the form $f = f(H, L_z)$ if we neglect individual collisions and treat only collective behaviour. The collisional effects will later be estimated at the steady state of the collisionless system.

For this paper we consider pseudo-Maxwellian distributions of the form

$$f(H, L_z) = n_0 \sqrt{\frac{2m}{2\pi^3 kT}} \exp\{-H/kT\} \exp\{-L_z^2/(2mr_0^2 kT)\} \times \operatorname{erfc}(\beta(H - H_c)/kT) \quad (3)$$

Here r_0 represents a characteristic radius at which angular momentum becomes significant; one might expect this to be of the order of the particle gyroradius. Spatial dependence is also implied through ϕ and A_θ and thus H . This form for the distribution, though very simple, will suffice to demonstrate the parameter-dependence of our

system. The gradient and value of the cutoff are determined by β and H_c respectively. Beyond this cutoff, particles are assumed to be able to escape from confinement. These pseudo-Maxwellian distributions can be expected to yield an underestimate for achievable fusion rate.

Recognising the symmetry between v_r and v_z in Eq. 3, we can rewrite it as

$$f_{\mathbf{v}}(v_L, v_\theta, A_\theta, \phi, r) = \frac{2n_0}{\sqrt{\pi}} \sqrt{\frac{m}{2kT}} v_L \times \exp \left\{ -\frac{m}{2kT} (v_L^2 + v_\theta^2 + \frac{2q\phi}{m}) \right\} \times \exp \left\{ -\frac{1}{2mkT} (r/r_0)^2 (mv_\theta + qA_\theta)^2 \right\} \times \operatorname{erfc} \left(\frac{\beta m}{2kT} (v_L^2 + v_\theta^2 + \frac{2q\phi}{m}) - \frac{\beta H_c}{kT} \right) \quad (4)$$

with $v_L^2 = v_r^2 + v_z^2$. In this (v_L, v_θ) velocity-space, the angle-averaged velocity difference between two points \mathbf{v}_1 and \mathbf{v}_2 is

$$\langle \mathbf{v}_1 - \mathbf{v}_2 \rangle = \sqrt{v_{1L}^2 + v_{2L}^2} \hat{\mathbf{v}}_L + (v_{1\theta} - v_{2\theta}) \hat{\mathbf{v}}_\theta \quad (5)$$

Changing scales to remove dimensions, let:

$$\begin{aligned} v &\rightarrow v' \equiv v / \sqrt{2kT/m} \\ \phi &\rightarrow \phi' \equiv \frac{e\phi}{kT} \\ H_c &\rightarrow H'_c \equiv \frac{H_c}{kT} \\ A_\theta &\rightarrow A'_\theta \equiv eA_\theta / \sqrt{2mkT} \\ r &\rightarrow r' \equiv r/r_0 \end{aligned}$$

Dropping the primes (we will now work in the rescaled quantities):

$$f_{\mathbf{v}}(v_L, v_\theta, A_\theta, \phi, r) = \frac{2n_0}{\sqrt{\pi}} v_L \exp \left\{ -(v_L^2 + v_\theta^2 + Z\phi) \right\} \times \exp \left\{ -r^2 (v_\theta + ZA_\theta)^2 \right\} \times \operatorname{erfc} \left(\beta \left\{ v_L^2 + v_\theta^2 + Z\phi - H_c \right\} \right) \quad (6)$$

with Z the atomic number (1 for a deuteron, -1 for an electron).

In the limit where $H_c \rightarrow \infty$, the density is given by

$$\begin{aligned} n(A_\theta, \phi, r) &= \int_{-\infty}^{\infty} dv_\theta \int_0^{\infty} dv_L \lim_{H_c \rightarrow \infty} f_{\mathbf{v}}(v_L, v_\theta, A_\theta, \phi, r) \\ &= \frac{n_0}{\sqrt{r^2 + 1}} \exp \left\{ - \left(Z^2 A_\theta^2 \frac{r^2}{r^2 + 1} + Z\phi \right) \right\} \end{aligned} \quad (7)$$

The presence of the cutoff complicates this somewhat; after some algebra and taking the limit $\beta \gg 1$, we arrive

at the approximate form, derived in appendix A:

$$\begin{aligned} \lim_{\beta \rightarrow \infty} n(A_\theta, \phi, r) &= \frac{\sqrt{\pi}}{2} \exp \left\{ -(rZA_\theta)^2 \right\} \left\{ \frac{1}{\tilde{r}} \exp \left\{ (r^4/\tilde{r}^2) Z^2 A_\theta^2 - Z\phi \right\} \mathcal{C} \left(\frac{r^2}{\tilde{r}} ZA_\theta, \tilde{r}w \right) \right. \\ &\quad \left. - \frac{1}{r} \exp \left\{ r^2 Z^2 A_\theta^2 - H_c \right\} \mathcal{C}(rZA_\theta, rw) \right\} \end{aligned} \quad (8)$$

where $w = \Re \left(\sqrt{H_c - Z\phi} \right) \geq 0$, $\tilde{r} = \sqrt{r^2 + 1}$ and $\mathcal{C}(a, b) = \operatorname{erf}(a + b) - \operatorname{erf}(a - b)$

Imaginary values for w are forbidden as they would represent plasma with potential energy beyond the energetic cutoff at H_c .

A sufficient condition for magnetic shielding is $\mathcal{C} \ll 1$ near the coil surface, i.e:

$$ZA_\theta > \left(w + \frac{1}{r} \right) \quad (9)$$

Eq. 9 is more readily satisfied as the device becomes larger.

Restoring dimensions, we can evaluate Eq. 9 along the plane of a coil at half the coil radius, using the approximation for a current loop of radius a [39]:

$$A_\theta(r = a/2, z = 0) \approx \left(\frac{4}{29} \right) \mu_0 I \quad (10)$$

After a small amount of algebra, Eq. 9 reduces to the following (in S.I.):

$$I > \frac{29\sqrt{2m} \left(\sqrt{H_c - q\phi_{\text{coil}}} + 2\sqrt{kT} \left(\frac{r_0}{r_{\text{coil}}} \right) \right)}{4\mu_0 q} \quad (11)$$

For a system of two opposed coils spaced approximately a radius apart, the current required differs from this by only a few percent. It is worth noting the scaling with the square root of energy.

Given the ion distribution f_i , fusion power is given by the standard expression

$$P_{\text{fus}} = \frac{1}{2} E_{\text{fus}} \int d^3x n_i(x)^2 \langle \sigma v \rangle, \quad (12)$$

where E_{fus} is the fusion energy and

$$\begin{aligned} \langle \sigma v \rangle &= (1/n_i(x)^2) \times \\ &\iint d\mathbf{v} \iint d\mathbf{v}' \|\langle \mathbf{v} - \mathbf{v}' \rangle\| \sigma(\|\langle \mathbf{v} - \mathbf{v}' \rangle\|) f_i(\mathbf{v}) f_i(\mathbf{v}'). \end{aligned} \quad (13)$$

To quantify the above we adopt the fit to the D-D fusion cross-section due to Duane [36].

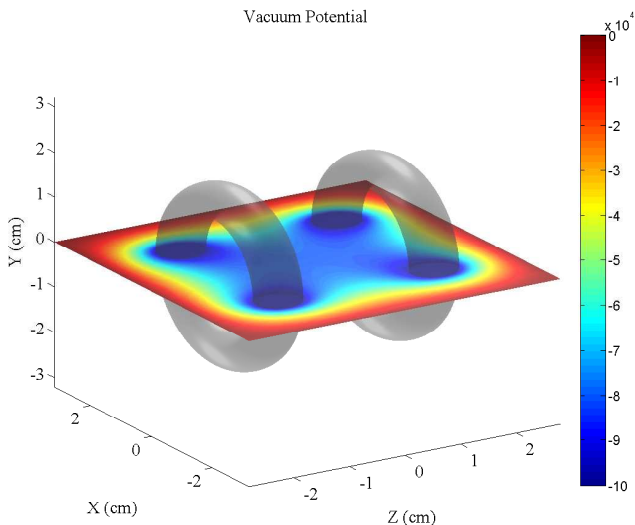


FIG. 3: Example Vacuum electric potential of charged cusp.

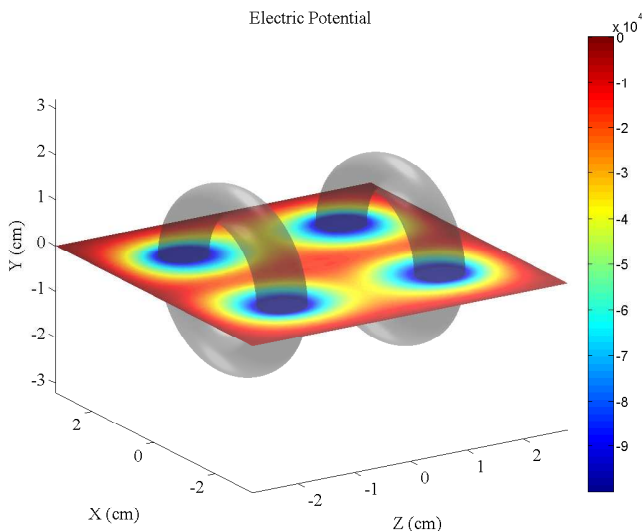


FIG. 4: Electric potential of example system with plasma present.

C. Cusp Losses

Since typical operation of an electromagnetic cusp device involves the formation of a central potential, we need to obtain the appropriate expressions for cusp confinement where an electric field is also present. For clarity, we work in S.I. in this section.

Derivation of the loss-cone angle begins with the force on a diamagnetic particle:

$$\mathbf{F}_{\parallel} = -\mu\nabla B - q\nabla\phi \quad (14)$$

Since charge is conserved, energy conservation yields the separate conservation of the magnetic moment μ .

We consider the motion of a particle turning around

between fields B_0, ϕ_0 and B', ϕ' . Let

$$\mathbf{v}_0 = \mathbf{v}_{\perp 0} + \mathbf{v}_{\parallel 0} \quad (15)$$

$$\mathbf{v}' = \mathbf{v}'_{\perp} \quad (16)$$

where \mathbf{v}_0 and \mathbf{v}' , respectively, are the velocities at B_0 and B' .

Energy and magnetic moment conservation, respectively, yield

$$\frac{1}{2}mv'_{\perp}{}^2 + q\phi' = \frac{1}{2}mv_0^2 + q\phi_0 \quad (17)$$

$$\frac{v_{\perp 0}^2}{B_0} = \frac{v'_{\perp}{}^2}{B'} \quad (18)$$

Combining and rearranging, we get

$$\frac{B_0}{B'} = \frac{v_{\perp 0}^2}{v_0^2 + \frac{2q}{m}(\phi_0 - \phi')} \quad (19)$$

which yields the corrected loss-cone angle as

$$\sin^2 \theta_m = \frac{B_0}{B_m} \left(1 + \frac{2q}{mv_0^2}(\phi_0 - \phi_m) \right) \equiv \frac{1}{R_m} \quad (20)$$

where θ is the angle between the velocity vector \mathbf{v}_0 and the magnetic field in the low-field region, and B_m is the maximum magnetic field strength encountered by the particle during its motion. If we can hold the coils at a negative potential with respect to the centre of the device, the combined electromagnetic trapping is sufficient to eliminate electron cusp losses for electrons of energy below a small multiple of the virtual anode height. Depending on the geometry, such a virtual anode can form naturally when the coils are held at a negative potential with respect to the boundary (e.g vacuum chamber).

D. Grid Losses

Since the magnetic field of a cusp is convex inward, both the curvature and ∇B drifts are nowhere towards the coils. We can prevent a particle from reaching the coils by insisting that the gyroradius becomes smaller than the distance of approach.

We recall the definition of the gyroradius

$$r_g = \frac{mv_{\perp}}{qB} \quad (21)$$

Approximating the magnetic field near the current-loops with that due to a line-segment of current, we have

$$B(s) = \frac{\mu_0 I}{2\pi s} \quad (22)$$

with s the perpendicular distance from the line-segment.

We require $r_g(r) < r - r_c$ for some r_c representing the thickness (minor radius) of the coils; solving for I yields:

$$I > \frac{2\pi m v_{\perp}}{\mu_0 q (1 - \frac{r_c}{r})} \approx \frac{2\pi \sqrt{2E_i m_i}}{\mu_0 q (1 - \frac{r_c}{r})} \quad (23)$$

Inspecting Eq. 23, we see that the required number of Ampere-turns depends on the achievable separation between metal surfaces. This suggests the use of coils with a small minor radius.

If we take $r' = 2r_c$ with r' the distance at which our condition applies, then the above simplifies to

$$I > \frac{4\pi \sqrt{2E_i m_i}}{\mu_0 q_i}. \quad (24)$$

We can rearrange Eq. 24 to find a critical energy for a given current, below which particles cannot escape to the grid:

$$E_{\text{crit}} = \frac{\mu_0^2 q_i^2 I^2}{32\pi^2 m_i} \quad (25)$$

The structure of this agrees with our earlier approach through the distribution function (Eq. 11).

If $E_{\text{crit}} > -q_i \phi_{\text{coil}}$, upscattered ions will be lost to the chamber walls before they are lost to the grid.

E. Bremsstrahlung

Bremsstrahlung is a significant loss mechanism for IEC systems; both efficiency and safety demand that our system does not radiate all the input energy as X-rays.

For electron-electron bremsstrahlung we can use the result of Gould [27, 28]:

$$\frac{P_{\text{brem,e,e}}}{V} = \frac{20(44 - 3\pi^2)}{9\sqrt{\pi}} \alpha^3 \left(\frac{\hbar}{mc}\right)^2 \sqrt{m_e} n_e^2 (kT_e)^{3/2} \quad (26)$$

with α the fine structure constant, T_e the electron temperature.

In the case where an ion species is in thermal equilibrium with the electrons, an expression for electron-ion bremsstrahlung power density, due once again to Gould is

$$\frac{P_{\text{brem,e,i,eq}}}{V} = \frac{32}{3} \sqrt{\frac{2}{\pi}} \alpha^3 \frac{\hbar^2 c}{m} n_e Z_i^2 n_i \tau \left(1 + \frac{11\tau}{24}\right) \quad (27)$$

with $\tau = kT_e/mc^2$.

In our device, the ions and electrons are not necessarily in thermal equilibrium. Where the ions are slower than the electrons, the effect on bremsstrahlung is small. Where the ions are faster than the electrons we can simply replace τ in the above with $\tau' = (T_i m_e / T_e m_i) \tau$ i.e. using the approximate electron temperature in the rest-frame of the ion as suggested by Jones [29]. The electron-ion Bremsstrahlung is computed using the larger of τ and τ' ; this selection is performed at each point in space.

F. Collisional up-scattering

Interspecies energy transfer and collisionally-induced upscattering both represent energy-loss mechanisms for an IEC-style device. We can obtain useful estimates of the magnitudes of such losses from the Landau equation for the scattering of particles of distribution f_a due to distribution f_b [35]:

$$\frac{\partial f_a(\mathbf{v})}{\partial t} = \frac{c_{ab}}{m_a} \nabla_{\mathbf{v}} \cdot \mathbf{J}(f_a, f_b, \mathbf{v})$$

with

$$\mathbf{J}(f_a, f_b, \mathbf{v}) = \int \int dv'_L dv'_\theta \left(\frac{\mathcal{I}}{u} - \frac{\mathbf{u}\mathbf{u}}{u^3} \right) \cdot \left[\frac{f_b(\mathbf{v}')}{m_a} \nabla_{\mathbf{v}} f_a - \frac{f_a(\mathbf{v})}{m_b} \nabla_{\mathbf{v}'} f_b \right] \quad (28)$$

where \mathcal{I} denotes the unit dyadic, $\mathbf{u}\mathbf{u}$ is the tensor product of \mathbf{u} with itself, and

$$c_{ab} = \frac{Z_a^2 Z_b^2 e^4 \ln(\Lambda)}{8\pi\epsilon_0^2} \quad (29)$$

$$\ln(\Lambda) = \ln(4\pi\epsilon_0 kT \frac{m_e}{m_a} \langle v_a^2 \rangle \lambda_D / q_e^2) \quad (30)$$

$$\mathbf{u} = \langle \mathbf{v} - \mathbf{v}' \rangle \quad (\text{c.f Eq.5}). \quad (31)$$

For our distribution, the derivatives are as follows:

$$\frac{\partial f}{\partial v_L} = \left[\frac{1}{v_L} - 2v_L (1 + K(H)) \right] f \equiv k_L f \quad (32)$$

and

$$\frac{\partial f}{\partial v_\theta} = -2 \left[v_\theta (1 + r^2 + K(H)) + r^2 Z A_\theta \right] f \equiv k_\theta f \quad (33)$$

where

$$K(H) = \frac{2\beta \exp\{-\beta^2(H - H_c)^2\}}{\sqrt{\pi} \operatorname{erfc}(\beta(H - H_c))} \quad (34)$$

with $H = v_L^2 + v_\theta^2 + Z\phi$. The term $K(H)$ is a pure consequence of our cutoff. Without such a cutoff, it is seen that upscattering and heating power may be dramatically underestimated.

Recalling that the average energy of a particle of species a is by definition

$$\langle E_a \rangle = \frac{1}{n} \int f(\mathbf{v}) E(\mathbf{v}) d^3\mathbf{v} \quad (35)$$

the total heating power experienced by species a is

$$P_{\text{heat, a}}(x) = n_a(x) \frac{\partial \langle E_a \rangle}{\partial t} = \int \int dv_L dv_\theta \frac{\partial f_a(\mathbf{v})}{\partial t} E(\mathbf{v}) \quad (36)$$

$$= -c_{ab} \int_{-\infty}^{\infty} dv_\theta \int_0^{\infty} dv_L \mathbf{v} \cdot \mathbf{J}(f_a, f_b, \mathbf{v}) \quad (37)$$

Here, use has been made of the product rule for continuously differentiable functions:

$$\int_{\Omega} \frac{\partial u}{\partial x_i} v d\Omega = \int_{\Gamma} uv \hat{\nu}_i d\Gamma - \int_{\Omega} u \frac{\partial v}{\partial x_i} d\Omega, \quad (38)$$

where Γ is the boundary of volume Ω . In each of our particular cases at least one of these terms vanishes.

Up-scattering-driven loss power can be computed in the same fashion with merely a change of integration limits such that we integrate over that region of the distribution holding particles that can escape and replace $E(\mathbf{v})$ with a bound on the kinetic energy at the chamber wall.

$$\begin{aligned} P_{\text{upscattering loss for species a}} &= \sum_b c_{ab} \int_{\infty}^{\infty} dv_{\theta} \times \\ & (v_{\theta}^2 + H_c) \hat{\nu}_L \cdot \mathbf{J}(f_a, f_b, \mathbf{v} = (w_a, v_{\theta})) \end{aligned} \quad (39)$$

Note that we remain in dimensionless units; to get power in Watts, we multiply the above by kT (expressed in Joules).

G. Power balance

Each fusion event consumes two ions. The number of fusion events per unit time is $R_{\text{fus}} = P_{\text{fus}}/E_{\text{fus}}$. Maintaining energy balance requires we replace fused ions with fresh ions at the pre-collision energy. Since this is necessarily less than the maximum ion kinetic energy, we can bound this by:

$$P_{\text{ion loss}} < P_{\text{ion upscattering loss}} + 2P_{\text{fus}} \frac{|q_i \phi_{\text{coil}}|}{E_{\text{fus}}} \quad (40)$$

Let $Q \equiv \frac{\text{Useful Power Out}}{\text{Power in}}$.

If the fraction of fusion power which can be captured is η_f then

$$\text{Useful Power Out} = \eta_f P_{\text{fusion}} \quad (41)$$

Power loss in the coils will be omitted under the assumption that a real fusion power system will employ superconducting magnets. We will treat only the case where ions exert a net heating effect on the electrons; we will then add the electron heating power to the electron loss power. The continuous power input required by a fusion system such as has been described is at most

$$\text{Power in} = P_{\text{brem}} + P_{\text{electron heating}} + P_{\text{ion loss}} + P_{\text{electron loss}} \quad (42)$$

Thus

$$Q = \frac{\eta_f P_{\text{fusion}}}{P_{\text{brem}} + P_{\text{electron heating}} + P_{\text{ion loss}} + P_{\text{electron loss}}} \quad (43)$$

The combined-cycle efficiency of a modern gas-turbine approaches 60% - we will thus take $\eta = 0.6$ as a representative choice.

Results

For this paper, we restrict ourselves to low densities; in particular, we ensure that the particle currents are small enough that we can use the vacuum values for the magnetic vector potential. Where this is true, we can solve iteratively for a self-consistent density and electrostatic potential structure by repeatedly recomputing densities and averaging the resulting ϕ . The electrostatic potential for a given density profile, coil potential, and grounded chamber is itself computed through an over-relaxation developed for this paper. When computing electron densities, the value H_c for the electron population has been continuously adjusted such that $Z\phi > H_c$ everywhere on the interior of the device and $Z\phi = H_c$ at at least one point on the boundary.

Electrons outside the device will be both fast-moving and rapidly lost to the walls. To model this, electron densities in the region exterior to the coils have been held at zero during the relaxation.

Once the potentials A_{θ} and ϕ have been obtained everywhere on our spatial lattice, numerically integrate is performed to compute the gain and loss terms introduced in Eqns. 37 and 39. In the process, we derive spatial maps of the various quantities.

The first configuration examined is an electron-free system exhibiting a virtual cathode in the centre of the device. Parameters for this device are in table I. The potential-well structure with and without plasma is shown in Figs. 5, 6, 7, and 8. A local virtual anode is formed, but the potential of this local anode is lower than any point on the boundary.

The corresponding ion density is shown in Fig. 9. It must be understood that these 3D pictures show a slice; the corresponding density integrated over the azimuthal angle is given in Fig. 10 showing the total contribution from different radii.

Azimuthally-integrated fusion density for this configuration is depicted in Fig.11. Most of the fusion occurs close to the axis and near the planes of the coils. With no electrons to contribute to Bremsstrahlung, the dominant energy loss mechanism is the upscattering of ions; this is shown to be insignificant. The gain of the system reduces to $0.6 \times 2.5 \text{ MeV} / 100 \text{ keV} = 15$ as shown in Table I.

Introducing electrons allows higher densities through cancellation of the space-charge due to the ions. Parameters for an example system are given in Table II. Bremsstrahlung power is by far the dominant loss mechanism in this system; one should expect the electrons in such a system to exhibit considerable cooling, reducing this loss. The proper treatment of this reduction is left to future work.

The potential-well structure in Figs. 14 and 15 exhibits a small secondary virtual cathode - the ‘‘Poissor’’ structure proposed by Hirsch [3]. The overall virtual anode is responsible for a great enhancement in electron confinement. Figs. 16 and 17 show the ion and electron densities, respectively. The formation of a jet-like structure is

Parameter	Value
Vacuum chamber radius	40 mm
Vacuum chamber length	70 mm
Coil major radius	20 mm
Coil minor radius	4 mm
Coil separation	35 mm
Coil current	700 kA-turns
Coil potential	-100 kV
kT (ions)	10 keV
r_0 (ions)	5 mm
β (ions)	100
H_c (ions)	0
E_{fus}	2.5 MeV
spatial resolution	0.5 mm
Computed Quantity	Value
Max. ion density	$4.7 \times 10^{16} \text{ m}^{-3}$
Total fusion rate	2650 / s
Total fusion power	1.06 nW
Ion upscattering power	$1.0 \times 10^{-23} \text{ W}$
Q	≈ 15

TABLE I: Parameters for an electron-free system with a virtual cathode

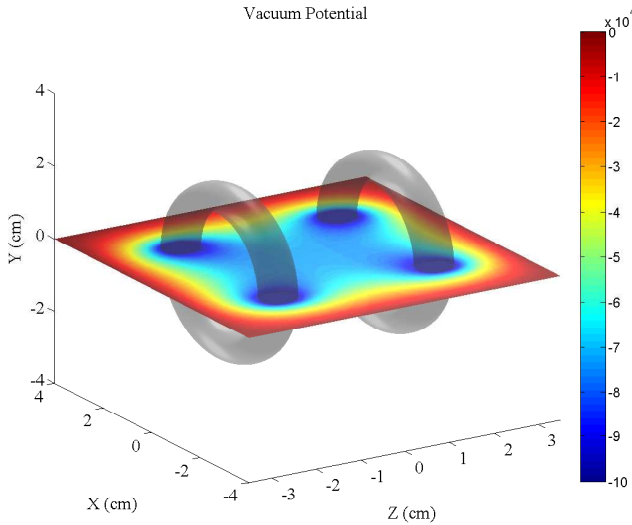


FIG. 5: Vacuum electric potential of electron-free virtual-cathode configuration

notable.

Fusion in this electron/ion configuration will occur in three rings, as show in Fig. 18. For a higher-density system, we would alter the geometry to raise the potential in the ring cusp and consequently shift more of the ion density towards the center of the system.

In both the cases depicted the gain, Q of the system is considerably greater than 1. No attempt has been made to optimise the parameters of the system; such a study awaits access to more computational power and extension

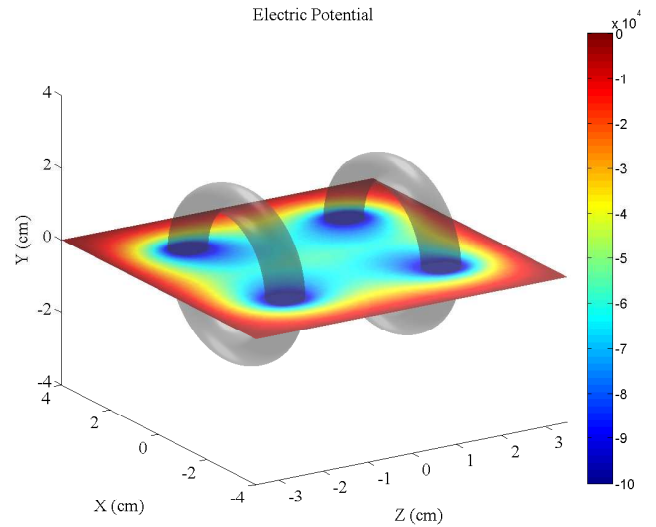


FIG. 6: Electric potential of virtual-cathode configuration with ions present

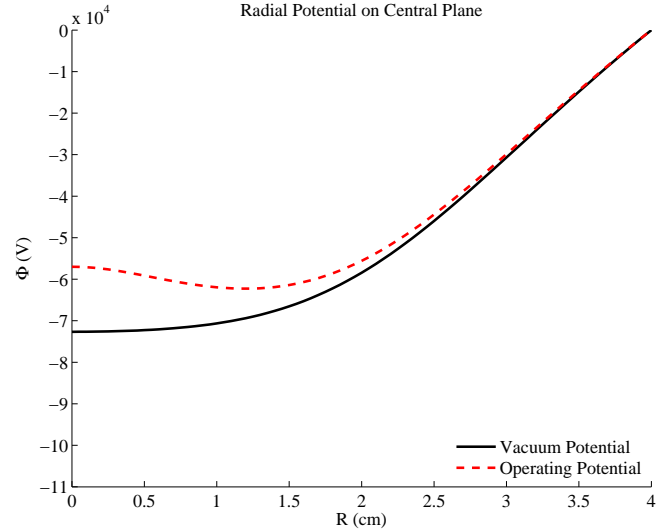


FIG. 7: Electric potential along a radial line through the midpoint of the device for electron-free configuration.

of the density/potential solver to higher densities where simple fixed-point iteration is no longer applicable.

Conclusions and Outlook

It has been shown that an IEC device can achieve energy gain if the electrodes are circular coils carrying sufficient current to prevent bombardment by and subsequent collection of charged particles. The required current can be estimated easily from the energy of the particles in the plasma. Gains of the order of 10 are predicted for a deuterium-burning system at low density. The combination of electric and magnetic potentials in this case is

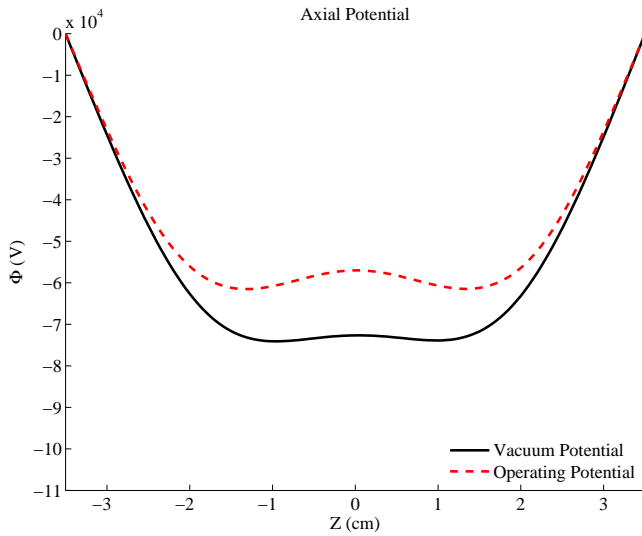


FIG. 8: Electric potential along an axial line through centre the device for electron-free configuration.

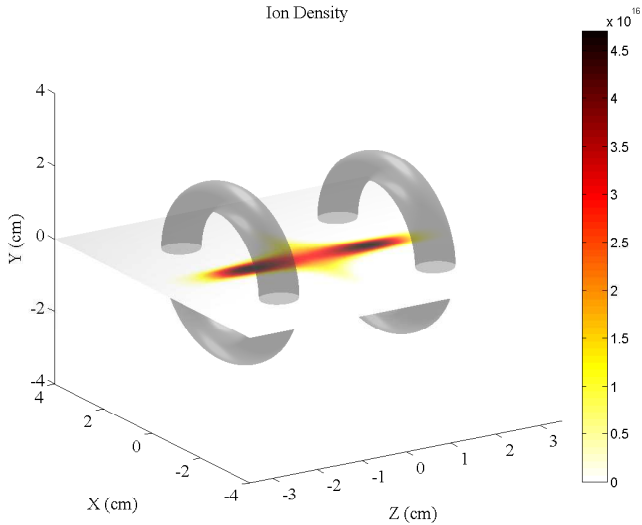


FIG. 9: 3D slice of ion density for the electron-free virtual-cathode configuration

sufficient to confine a significant electron population close to the device axis, admitting the possibility of a beam-like plasma with recirculating ions. The dimensions were chosen for numerical convenience - they should not be taken as representing limits to energy output. We see no reason why the device should not scale to MW outputs, with achievable fusion power bounded by thermal and mechanical properties of the materials used in construction.

Our results contrast with earlier work by Rider [33], whose conclusions we regard as dubious, and which cannot be recovered unless we assume a Maxwellian, quasineutral plasma with the density distribution due to Krall (derived for non-Maxwellian distribution) and ne-

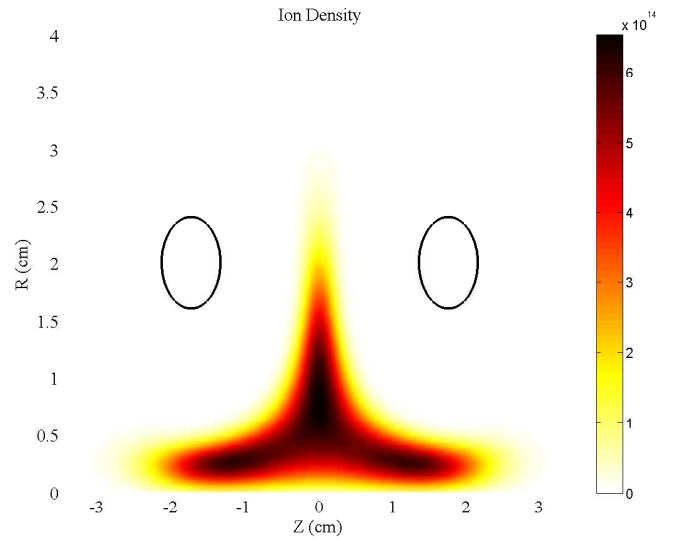


FIG. 10: Ion density in integrated (r,z) space for electron-free virtual-cathode configuration. Black circles show the coil cross-section.

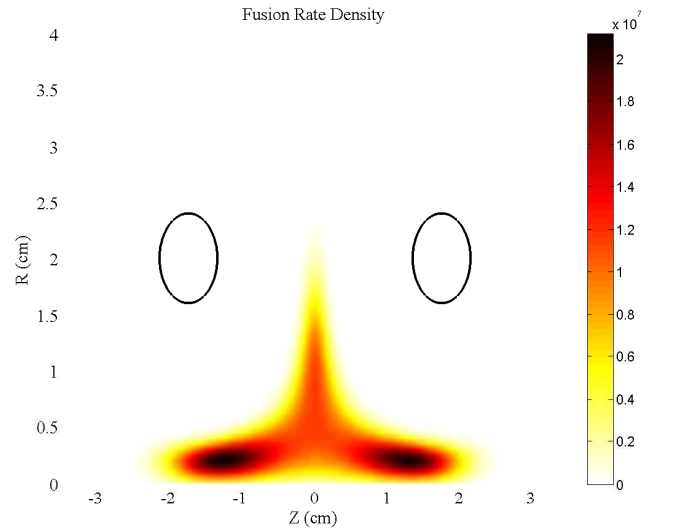


FIG. 11: Fusion-rate density in integrated (r,z) space for electron-free virtual-cathode configuration. Black circles show the coil cross-section; most of the fusion is occurring on the axis near the planes of the coils.

glect the use of the electrostatic potential for the mitigation of cusp losses. We are unable to imagine an IEC device consistent with all of Rider's assumptions; indeed concerns over self-consistency motivated much of our work.

Some caveats apply; we have deliberately ignored turbulence and instabilities; we have also ignored drifts which can arise through inhomogeneities in the plasma such as the diamagnetic drift. We quote results only for low densities of the order of mTorr and for power outputs in the nanoWatts. We have also assumed a form for

Parameter	Value
Vacuum chamber radius	40 mm
Vacuum chamber length	70 mm
Coil major radius	16 mm
Coil minor radius	4 mm
Coil separation	28 mm
Coil current	500 kA-turns
Coil potential	-100 kV
kT (ions, electrons)	10 keV
r_0 (ions, electrons)	5 mm
β (ions, electrons)	100
H_c (ions)	0
H_c (electrons)	20.9 keV
E_{fus}	2.5 MeV
spatial resolution	0.25 mm
Computed Quantity	Value
Max. ion density	$1.86 \times 10^{17} \text{ m}^{-3}$
Max. electron density	$2.04 \times 10^{17} \text{ m}^{-3}$
Total fusion rate	42360 / s
Total fusion power	17 nW
Total Brem power	0.4 nW
Electron upscattering power	$2.7 \times 10^{-4} \text{ nW}$
Electron heating power	$7 \times 10^{-4} \text{ nW}$
Ion upscattering power	$2.7 \times 10^{-9} \text{ nW}$
Ion upscattering power	$1.0 \times 10^{-23} \text{ W}$
Q	≈ 9

TABLE II: Parameters for an electron/ion system with a virtual anode

the distribution which corresponds to a steady state of the Vlasov equation and thus also ignore the dynamics of the approach to equilibrium - the steady state of a driven system should not be expected to be identical to this.

In adopting the Landau integral form for collisional transport, we are emphasising grazing collisions over strong collisions. In practice, all fusion systems must exhibit strong, inelastic, collisions - otherwise they would produce no fusion. The proper treatment of collisions for our system should involve a deeper consideration of these scattering events; one approach might be a monte-Carlo simulation involving full electrodynamics.

Finally, we have assumed a fully-ionized system. A real fusion system will include neutral species; ionization and recombination will introduce a new loss mechanism. As very high levels of ionization can be achieved at the low densities explored in this paper, we leave the exploration of the neutral-species interactions for another paper.

Future work will investigate the transition from the low- β regime to the high-beta cusp-confinement regime treated in other papers, and develop further the theory of plasma confinement in charged multipole cusps. It would be interesting to map the parameter-space boundary wherein $Q > 1$. The modest volume and density

requirements to produce measurable fusion rates suggest the cost of building an experimental device may not be prohibitive, either.

III. ACKNOWLEDGEMENTS

John Hedditch would like to thank Duncan and Annelies Hedditch for supporting him in this work, and David Gummersall for valuable discussion.

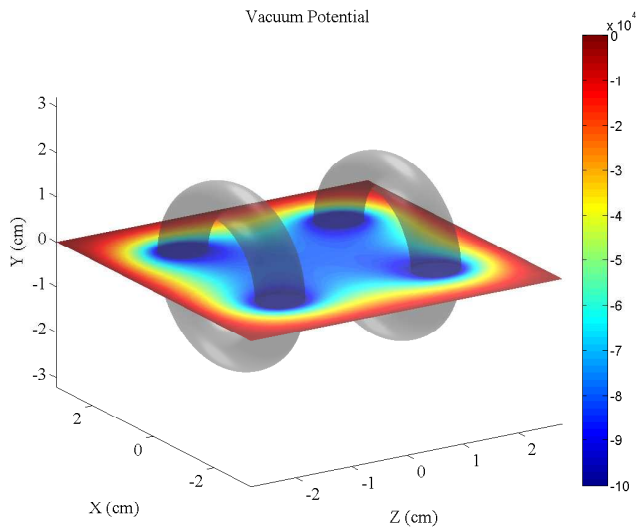


FIG. 12: Vacuum electric potential of electron/ion system

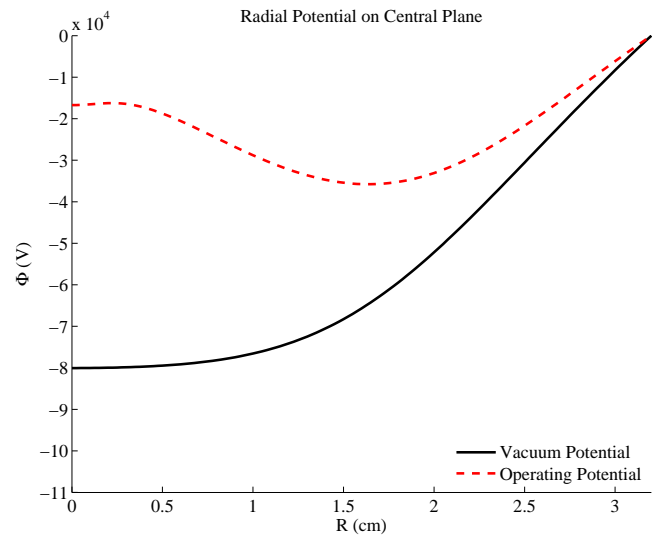


FIG. 14: Electric potential along a radial line through the midpoint of the device where electrons are present.

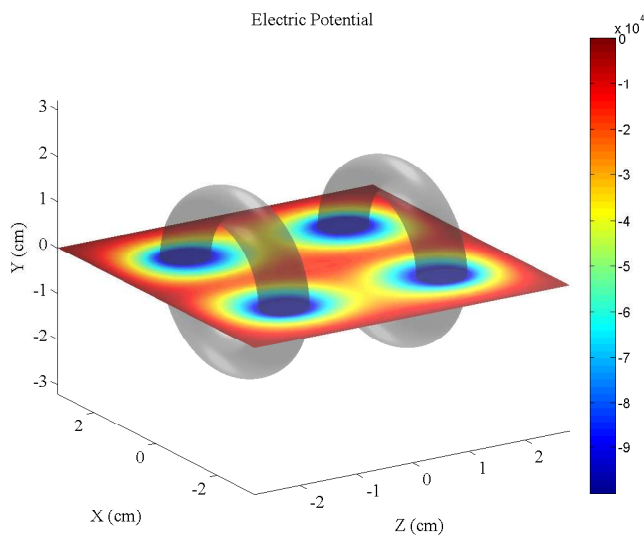


FIG. 13: Electric potential of electron/ion system with plasma present

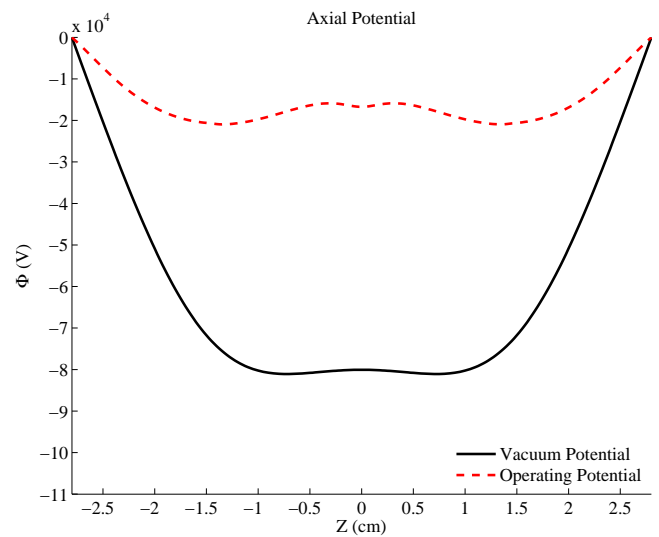


FIG. 15: Electric potential along an axial line through centre the device where electrons are present.

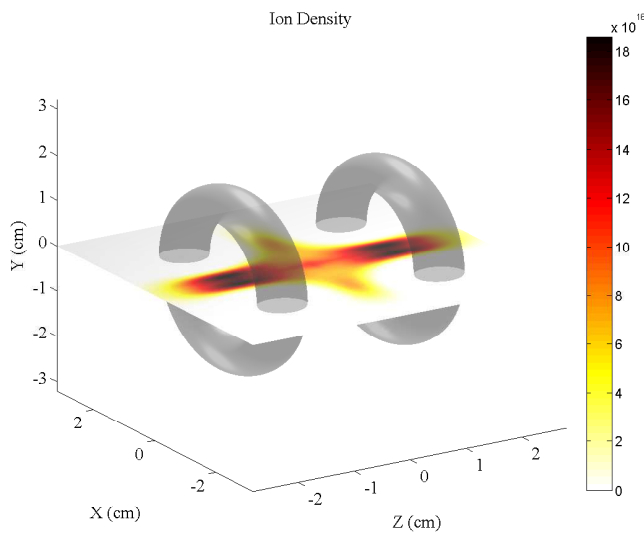


FIG. 16: Ion density in the electron/ion system

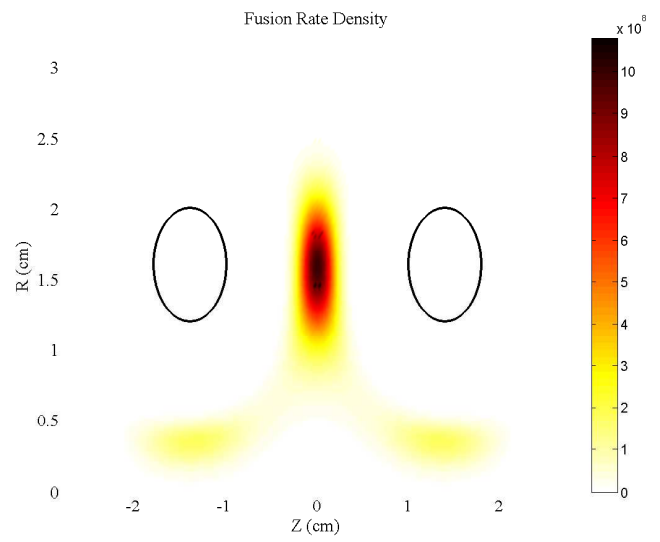


FIG. 18: Fusion rate density in the electron/ion system

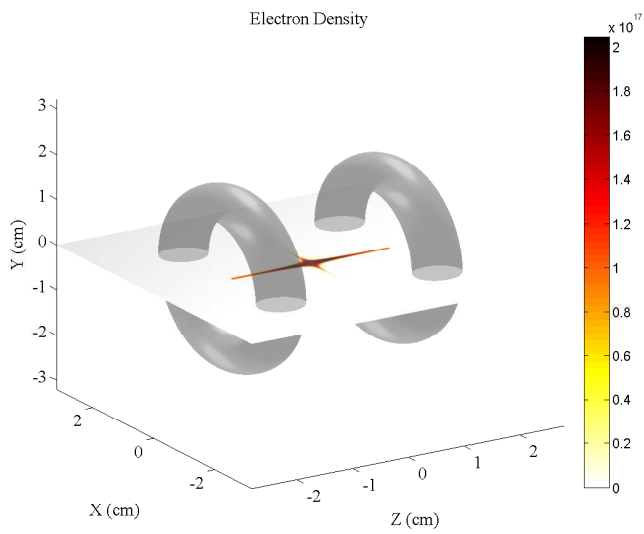


FIG. 17: Electron density in the electron/ion system

-
- [1] P. T. Farnsworth, U.S. Patent No. 3,258,402 (1966).
- [2] P. T. Farnsworth, U.S. Patent No. 3,386,883 (1968).
- [3] R. L. Hirsch, J. Appl. Phys. **38**, 4522 (1967).
- [4] R. L. Hirsch, Phys. Fluids **11**, 2486 (1968).
- [5] W. C. Elmore, J. L. Tuck, and K. M. Watson, Phys. Fluids **2**, 239 (1959).
- [6] O. A. Lavrentev, Ukr. Fiz. Zh. **8**, 440 (1963).
- [7] K. Yoshikawa et al, Nuclear Fusion **41** 6 (2001).
- [8] G. H. Miley, J. Nadler, T. Hochberg, Y. Gu, O. Barnouin, and J. Lovberg, Fusion Technol. **19**, 840 (1991).
- [9] G. H. Miley and J. Sved, Applied Radiation and Isotopes **48** 10 (1997)
- [10] D. C. Barnes, R. A. Nebel, and Leaf Turner, Phys. Fluids B **5**, 3651 (1993).
- [11] J. Park, R. A. Nebel, and S. Stange, Phys. Rev. Lett. **95**, 015003 (2005).
- [12] C. Tuft and J. Khachan, Phys. Plasmas **17**, 112117 (2010).
- [13] R. Bandara and J. Khachan, Phys. Plasmas **20**, 072705 (2013).
- [14] Nicholas A. Krall, M. Coleman, K. Maffei, J. Lovberg, FL Jacobsen, R. W. Bussard, Phys. Plasmas **2**, 146 (1995).
- [15] Matthew Carr and Joe Khachan, Phys. Plasmas **17**, 052510 (2010).
- [16] Matthew Carr, David Gummertsall, Scott Cornish, and Joe Khachan, Phys. Plasmas **18**, 112501 (2011).
- [17] Matthew Carr and Joe Khachan, Phys. Plasmas **20**, 052504 (2013).
- [18] S. Cornish,a) D. Gummertsall, M. Carr, and J. Khachan, Phys. Plasmas **21**, 092502 (2014).
- [19] J. Khachan and S. Collis, Phys. Plasmas **8**, 1299 (2001).
- [20] J. Khachan, D. Moore, and S. Bosi, Phys. Plasmas **10**, 596 (2003).
- [21] O. Shrier, J. Khachan, S. Bosi, M. Fitzgerald, and N. Evans, Phys. Plasmas **13**, 012703 (2006).
- [22] Nicholas A Krall, Fusion Technology, **22**, 42 (1992).
- [23] S. Chandrasekhar, Astrophys. J. **97**, 255 (1943).
- [24] Subrahmanyam Chandrasekhar, *Principles of stellar dynamics* (Courier Dover Publications, 2005).
- [25] Francis F Chen, *Introduction to plasma physics and controlled fusion volume 1: Plasma physics* (Plenum Press, New York, 1984).
- [26] S. Glasstone and R.H. Lovberg, *Controlled ther- monuclear reactions* (D. Van Nostrand Company, New York, 1960).
- [27] R. J. Gould, Astrophys. J. **238**, 1026 (1980).
- [28] R. J Gould, Astrophys. J., **243**, 677 (1981).
- [29] Frank C Jones, Astrophys. J., **169**, 503 (1971).
- [30] Kenro Miyamoto, *Fundamentals of plasma physics and controlled fusion*, Technical report, National Inst. for Fusion Science, Toki, Gifu (Japan), (2011).
- [31] W.M. Nevins and R. Swain, Nuclear fusion, **40**, 865 (2000).
- [32] K Nishimura, Phys. Lett. A, **38**, 535 (1972).
- [33] T.H Rider, Phys. Plasmas, **2**, 1853 (1995).
- [34] L. Spitzer Jr, *Physics of fully ionized gases*, (Interscience, New York, 1962).
- [35] V.M. Zhdanov, *Transport Processes in Multicomponent Plasma*, (CRC Press, 2002).
- [36] B.H. Duane, *Fusion Cross Section Theory, Rept. BNWL-1685*, (Brookhaven National Laboratory, 1972)
- [37] T.J. Dolan, Plasma Phys. Control. Fusion **36**, 1539 (1994)
- [38] A.S. Kaye J. Plasma Phys. **11**, 77 (1974)
- [39] J.D. Jackson, *Classical Electrodynamics*, (Wiley, New York, 1975)

Here we present the derivation of the density for our distribution away from the limit of infinitely-sharp cutoff.

Appendix A: Density calculation

Using the fact that

$$\int dx x e^{-x^2/c} \operatorname{erfc}(ax^2 + b) = -\frac{c}{2} e^{-\frac{x^2}{c}} \left\{ e^{\left(\frac{x^2}{c} + \frac{b}{ac} + \frac{1}{4a^2c^2}\right)} \operatorname{erf}\left(ax^2 + b + \frac{1}{2ac}\right) + \operatorname{erfc}(ax^2 + b) \right\} + C \quad (\text{A1})$$

we have

$$\int_0^\infty dx x e^{-x^2/c} \operatorname{erfc}(ax^2 + b) = \frac{c}{2} \left\{ \operatorname{erfc}(b) - e^{\left(\frac{b}{ac} + \frac{1}{4a^2c^2}\right)} \operatorname{erfc}\left(b + \frac{1}{2ac}\right) \right\} \quad (\text{A2})$$

and therefore

$$\int_0^\infty dv_L F_L(v_L, v_\theta, \phi) = \frac{1}{2} \left\{ \operatorname{erfc}(\beta C(v_\theta, \phi)) - \exp\left\{C(v_\theta, \phi) + \frac{1}{4\beta^2}\right\} \operatorname{erfc}\left(\beta C(v_\theta, \phi) + \frac{1}{2\beta}\right) \right\} \quad (\text{A3})$$

where

$$C(v_\theta, \phi) = v_\theta^2 + Z\phi - H_c = (H - H_c)|_{v_L=0}$$

The density integral then reduces to

$$\begin{aligned} n(A_\theta, \phi, r) = \frac{1}{2} e^{-(ZA_\theta r)^2} & \left\{ e^{-Z\phi} \int_{-\infty}^\infty dv_\theta e^{-r^2(v_\theta^2 + 2Zv_\theta A_\theta)} e^{-v_\theta^2} \operatorname{erfc}(\beta \{v_\theta^2 + Z\phi - H_c\}) \right. \\ & \left. - e^{\frac{1}{4\beta^2}} e^{-H_c} \int_{-\infty}^\infty dv_\theta e^{-r^2(v_\theta^2 + 2Zv_\theta A_\theta)} \operatorname{erfc}\left(\beta \{v_\theta^2 + Z\phi - H_c\} + \frac{1}{2\beta}\right) \right\} \end{aligned} \quad (\text{A4})$$

We can approximate these integrals as follows:

$$\int_{-\infty}^\infty f(x) \operatorname{erfc}(g(x^2)) dx \approx 2 \int_{-v_-}^{v_-} f(x) dx + \int_{-v_+}^{-v_-} \left(1 - \frac{2g(x^2)}{\sqrt{\pi}}\right) f(x) dx + \int_{v_-}^{v_+} \left(1 - \frac{2g(x^2)}{\sqrt{\pi}}\right) f(x) dx \quad (\text{A5})$$

where

$$v_\pm = \Re(z_\pm) \mid g(z_\pm^2) = \pm \frac{\sqrt{\pi}}{2} \quad (\text{A6})$$

This yields the following expression for the density:

$$\begin{aligned} n(A_\theta, \phi, r) = e^{-(ZA_\theta r)^2} & \left\{ e^{-Z\phi} [J(v_-) + I(-v_-) - I(-v_+) + I(v_+) - I(v_-)] \right. \\ & \left. - e^{\frac{1}{4\beta^2}} e^{-H_c} [J'(v'_-) + I'(-v'_-) - I'(-v'_+) + I'(v'_+) - I'(v'_-)] \right\} \end{aligned} \quad (\text{A7})$$

where

$$\begin{aligned} v_\pm &= \Re \left(\sqrt{\pm \frac{\sqrt{\pi}}{2\beta} + H_c - Z\phi} \right) \\ v'_\pm &= \Re \left(\sqrt{\pm \frac{\sqrt{\pi}}{2\beta} + H_c - Z\phi - \frac{1}{2\beta^2}} \right) \end{aligned} \quad (\text{A8})$$

$$J(v) = \frac{\sqrt{\pi}}{\tilde{r}} e^{\frac{(r^2 Z A_\theta)^2}{\tilde{r}^2}} \left[\operatorname{erf} \left(\frac{\tilde{r}^2 v + r^2 Z A_\theta}{\tilde{r}} \right) - \operatorname{erf} \left(\frac{r^2 Z A_\theta - \tilde{r}^2 v}{\tilde{r}} \right) \right] \quad (\text{A9})$$

$$\begin{aligned} I(v) &= \frac{\exp \{ -(\tilde{r}^2 v^2 + 2r^2 Z A_\theta v) \}}{4\sqrt{\pi}\tilde{r}^5} \\ &\times \left\{ \sqrt{\pi} \exp \left\{ (\tilde{r}^2 v + r^2 Z A_\theta)^2 / \tilde{r}^2 \right\} \operatorname{erf} \left(\frac{\tilde{r}^2 v + r^2 Z A_\theta}{\tilde{r}} \right) \left[2\tilde{r}^2 (\sqrt{\pi} - 2\beta (Z\phi - H_c)) - 2\tilde{r}^2 \beta - \beta(2r^2 Z A_\theta)^2 \right] \right. \\ &\quad \left. + 2\tilde{r}\beta [2\tilde{r}^2 v + 2r^2 Z A_\theta] \right\} \end{aligned} \quad (\text{A10})$$

$$\begin{aligned} I'(v') &= \frac{\exp \{ -(r^2 v'^2 + 2r^2 Z A_\theta v') \}}{4\sqrt{\pi}r^5} \\ &\times \left\{ \sqrt{\pi} \exp \left\{ (r^2 v' + r^2 Z A_\theta)^2 / r^2 \right\} \operatorname{erf} \left(\frac{r^2 v' + r^2 Z A_\theta}{r} \right) \left[2r^2 \left(\sqrt{\pi} - 2\beta (Z\phi - H_c) - \frac{1}{\beta} \right) - 2r^2 \beta - \beta(2r^2 Z A_\theta)^2 \right] \right. \\ &\quad \left. + 2r\beta [2r^2 v' + 2r^2 Z A_\theta] \right\} \end{aligned} \quad (\text{A11})$$

$$J'(v') = \frac{\sqrt{\pi}}{r} e^{(r Z A_\theta)^2} [\operatorname{erf} (r v' + r Z A_\theta) - \operatorname{erf} (r Z A_\theta - r v')] \quad (\text{A12})$$

and $\tilde{r} = \sqrt{r^2 + 1}$.
